GIScience & Remote Sensing
Publication details, including instructions for authors and subscription information:
http://www.tandfonline.com/loi/tgrs20

Landfast sea ice monitoring using multisensor fusion in the Antarctic

Miae Kim[a], Jungho Im[a], Hyangsun Han[a], Jinwoo Kim[ab], Sanggyun Lee[a], Minso Shin[a] & Hyun-Cheol Kim[c]

[a] School of Urban and Environmental Engineering, Ulsan National Institute of Science and Technology, Ulsan, South Korea

[b] Space Imaging R&D Lab, LIG Nex1 Co., Ltd., Yongin, South Korea

[c] Division of Polar Ocean Environment, Korea Polar Research Institute, Incheon, South Korea

Published online: 31 Mar 2015.

To cite this article: Miae Kim, Jungho Im, Hyangsun Han, Jinwoo Kim, Sanggyun Lee, Minso Shin & Hyun-Cheol Kim (2015) Landfast sea ice monitoring using multisensor fusion in the Antarctic, GIScience & Remote Sensing, 52:2, 239-256, DOI: 10.1080/15481603.2015.1026050

To link to this article: http://dx.doi.org/10.1080/15481603.2015.1026050

GIScience & Remote Sensing, 2015
Vol. 52, No. 2, 239–256, http://dx.doi.org/10.1080/15481603.2015.1026050

Landfast sea ice monitoring using multisensor fusion in the Antarctic

Miae Kim[a], Jungho Im[a]*, Hyangsun Han[a], Jinwoo Kim[a,b], Sanggyun Lee[a], Minso Shin[a] and Hyun-Cheol Kim[c]

[a]*School of Urban and Environmental Engineering, Ulsan National Institute of Science and Technology, Ulsan, South Korea;* [b]*Space Imaging R&D Lab, LIG Nex1 Co., Ltd., Yongin, South Korea;* [c]*Division of Polar Ocean Environment, Korea Polar Research Institute, Incheon, South Korea*

(*Received 26 May 2014; accepted 28 February 2015*)

Landfast sea ice (fast ice) means sea ice that is attached to the shoreline with little or no motion in contrast to pack ice which drifts on the sea. As fast ice plays an important role in the environmental and biological systems of the Antarctic, it is crucial to accurately monitor the spatiotemporal distribution of fast ice. Previous studies on fast ice using satellite remote sensing were mostly focused on the Arctic and near-Arctic areas, whereas few studies were conducted over the Antarctic, especially the West Antarctic region. This research mapped fast ice using multisensor data from 2003 to 2008 based on machine learning approaches – decision trees (DTs) and random forest (RF). A total of seven satellite-derived products, including Advanced Microwave Scanning Radiometer for the Earth observing system brightness temperatures and sea ice concentration, Moderate Resolution Imaging Spectroradiometer (MODIS) ice surface temperature (IST) and Special Sensor Microwave/Imager ice velocity, were used as input variables for identifying fast ice. RF resulted in better performance than that of DT for fast ice classification. Visual comparison of the fast ice classification results with 250-m MODIS images for selected areas also revealed that RF outperformed DT. Ice velocity and IST were identified as the most contributing variables to classify fast ice. Spatiotemporal variations of fast ice in the East and West Antarctic were also examined using the time series of the fast ice maps produced by RF. The residence time of fast ice was much shorter in the West Antarctic than in the East.

Keywords: landfast sea ice; Antarctic; random forest; decision trees

1. Introduction

Landfast sea ice (hereafter fast ice) in the Antarctic is fastened to the coastline or the seaward edge of floating glaciers, as distinct from pack ice which drifts freely on the sea surface. The spatial distribution of fast ice and its temporal variation are closely related with the physical and environmental systems of the Antarctic. The variability of melt onset and freeze-up of fast ice is strongly correlated with changes in seawater and surface air temperature, wind speed, and precipitation on the ice surface such as snow accumulation (Heil 2006). An increase in the maximum thickness of fast ice corresponds to a decrease in oceanic heat flux (Heil, Allison, and Lytle 1996). Moreover, fast ice can play an important role in the marine ecosystems of the Antarctic Ocean. It has been reported that fast ice provides an extensive habitat for many organisms ranging from bacteria to

*Corresponding author. Email: ersgis@unist.ac.kr

various marine bird and mammal species, for example, successful breeding places for Emperor penguins and Weddell seals (Massom et al. 2009). Therefore, it is very important to monitor the spatial distribution and temporal variation of the properties of the Antarctic fast ice such as its extent and thickness.

Monitoring of the Antarctic fast ice has been conducted using *in situ* observations (Fedotov, Cherepanov, and Tyshko 1998; Heil 2006; Heil, Allison, and Lytle 1996; Lei et al. 2010; Tang et al. 2007) and satellite remote sensing (Fraser et al. 2012; Giles, Massom, and Lytle 2008; Massom et al. 2010; Fraser, Massom, and Michael 2009, 2010; Fraser 2011; Mahoney et al. 2007). Spatial distribution and thickness of the fast ice in Prydz Bay, East Antarctica, were investigated by the Antarctic Fast Ice Network project, a representative research program of *in situ* observations of the Antarctic fast ice promoted by Antarctic Climate & Ecosystems during the period of 1950–2021 (Heil, Gerland, and Granskog 2011). However, *in situ* observations have limitations in spatial continuous monitoring of the fast ice over vast areas at a continental scale.

Satellite remote sensing can be used as an alternative way of monitoring fast ice as it covers vast areas with high temporal resolution. Satellite-based research on fast ice can be divided into three categories in terms of sensor types by optical, active microwave, and passive microwave sensors. Optical sensors such as Landsat, the Moderate Resolution Imaging Spectroradiometer (MODIS), and the Advanced Very High Resolution Radiometer (AVHRR) have low and medium spatial resolution from dozens of meters to a few kilometers, while they observe the same area at least every other day (except the Landsat series). Fraser, Massom, and Michael (2009) used thermal infrared (TIR) and visible MODIS data to produce cloud-free composite images for fast ice detection at the Mertz Glacier Tongue, East Antarctica. Cloud-free TIR/visible AVHRR images were used for investigating the distribution and variations of fast ice along the Adélie coast, East Antarctica (Massom et al. 2009). However, optical sensors have limitations including the fact that they cannot observe the surface under cloudy sky or at night.

Microwave sensors have provided high-quality images independent of weather conditions and sun illumination. Synthetic aperture radar (SAR), an active microwave sensor, has observed surface properties with high spatial resolution of a few meters. Meyer et al. (2011) detected the seaward fast ice edge in Arctic regions using the interferometric technique with L-band SAR data. The fast ice edge was also delineated using Radarsat SAR images in northern Alaska and northwestern Canada (Mahoney et al. 2007). Giles, Massom, and Lytle (2008) created a distribution map of fast ice in part of the East Antarctica using an image correlation method with Radarsat ScanSAR imagery. Despite their advantages, it is difficult to investigate sea ice at a continental or global scale using active microwave sensors due to their narrow observation area.

Passive microwave sensors such as the Advanced Microwave Scanning Radiometer for the Earth observing system (AMSR-E), the Special Sensor Microwave/Imager (SSM/I), and the Special Sensor Microwave Imager/Sounder (SSMIS) can be successfully utilized for global-scale research on sea ice. Passive microwave sensors measure the surface radiation properties in various channels, such as sea ice concentration and sea ice velocity, with low spatial resolution of a few kilometers. Nevertheless, the passive microwave sensors can be successfully utilized for time series monitoring of sea ice at a global scale because they observe the entire Arctic and Antarctic areas every day. Tamura et al. (2007) monitored fast ice using SSM/I brightness temperature data to detect coastal polynyas in four sectors around the Antarctic coast.

As optical and microwave sensors have distinct strengths and weaknesses, several researchers have tried to fuse the strengths of each sensor for mapping the fast ice over a

wide area. Fraser, Massom, and Michael (2009) suggested a method of time series compositing cloud-free imagery from MODIS to detect fast ice in the East Antarctic, in which brightness temperature and concentration of sea ice derived by SSM/I with 25-km spatial resolution were used to define the extent of fast ice. Fraser, Massom, and Michael (2010) improved the accuracy of fast ice detection by replacing the products derived by SSM/I with those by AMSR-E, of which the spatial resolution is 6.25 km. Ushio (2006) analyzed the distribution and variations of fast ice in Lützow-Holm Bay, East Antarctica, with a time series of TIR images from AVHRR data and *in situ* measurements. The distribution of pack ice was determined with sea ice concentration data from SSM/I images.

While some studies were conducted to map and explore fast ice in the East Antarctic, few were performed over West Antarctica. Thus, this research aims at mapping and monitoring fast ice over the entire Antarctic area using time series satellite data. The objectives of this study are to (1) develop an automated model based on machine learning approaches for mapping fast ice through the synergistic use of time series optical and passive microwave data-sets for the entire Antarctic area, (2) explore accuracy patterns of the time series mapping results, (3) examine important variables for fast ice identification by model and how they affect the fast ice mapping results, (4) compare fast ice mapping results with the manually extracted fast ice edges from 250-m MODIS images for specific regions of interest, and (5) analyze the spatiotemporal variations of the Antarctic fast ice.

2. Data and methods

2.1. Data-set

2.1.1. Fast ice reference data

Fast ice maps of the East Antarctica from 2003 to 2008 produced by Fraser, Massom, and Michael (2010) were used as a reference data-set (Table 1). The reference maps were generated from 20-day composites of MODIS imagery in which cloud-covered areas were removed using the MOD35 cloud mask products (Fraser, Massom, and Michael 2009, 2010). Fast ice adjacent to the entire East Antarctic coastline was extracted using the MODIS composite images based on manual digitization with the help of AMSR-E sea ice concentration data (Fraser, Massom, and Michael 2010). The detailed procedures for deriving the reference data are described in Fraser, Massom, and Michael (2009, 2010).

2.1.2. Passive microwave data

Brightness temperature and sea ice concentration data from AMSR-E were used in this study (Table 1) (Cavalieri, Markus, and Comiso 2014). Since fast ice has radiative properties distinctive from pack ice due to emissivity difference, the brightness temperature measured by passive microwave sensors such as SSM/I and AMSR-E can be used as powerful tools to identify sea ice types. SSM/I measures vertically and horizontally polarized brightness temperature at 19.35, 37.0, and 85.5 GHz and vertically polarized brightness temperature only at 22.235 GHz. AMSR-E is composed of six frequencies: 6.925, 10.65, 18.7, 23.8, 36.5, and 89.0 GHz (Spreen, Kaleschke, and Heygster 2008; Comiso, Cavalieri, and Markus 2003). All frequencies of the AMSR-E instrument measure both vertically and horizontally polarized brightness temperature, which enables

a more detailed analysis of the physical properties of sea ice than the SSM/I-derived brightness temperature. The brightness temperature data measured at the 18.7, 23.8, 36.5, and 89.0 GHz channels of AMSR-E from 2003 to 2008 were used. Those channels are very effective for differentiating the radiative properties depending on sea ice types because of the dependency of polarization and spectral properties of the channels on emissivity differences (Cavalieri 1991).

The passive microwave sensors have provided sea ice concentration every day within a few tens of kilometers. As fast ice forms over a wide area attached to the coastlines, sea ice concentration of the fast ice is about 100%. Over pack ice areas, passive microwave sensors observe brightness temperature from both ice and open water, which results in low sea ice concentration. AMSR-E daily sea ice concentration over the Antarctic from 2003 to 2008 was used. The grid spacing of AMSR-E sea ice concentration is 12.5 km which is finer than that of SSM/I sea ice concentration of 25 km. Sea ice velocity derived by SSM/I was also used to classify the ice types (Table 1) (Fowler, Emery, and Tschudi 2013). The motion of fast ice is very small because it is fixed at the coastline or shallow seabed, while pack ice may move considerably in a short time period as the ice drifts freely by ocean current and wind.

2.1.3. *Optical sensor data*

Fast ice and pack ice have different physical properties such as snow depth on ice surface, ice thickness, and surface wetness, which determine the ice surface temperature (IST) (Hall et al. 2004). This means that the surface temperature of sea ice can be used as a variable to classify sea ice into fast ice and pack ice. The daily IST with 4-km spatial resolution measured by MODIS (MOD29E1D product) from 2003 to 2008 was used in this study (Table 1) (Hall, Salomonson, and Riggs 2006). Although MODIS IST is also provided with 1-km resolution, the aggregated 4-km IST data were used considering the spatial resolution of the other input variables, data processing time, and computational demand as the study area covers the entire Antarctic. Daily sea ice reflectance from the MOD29E1D product between 2003 and 2008 was used to define the extent of sea ice and to mask the open water area.

Table 1. Input variables and reference data information.

Satellite sensors	Variables	Spatial resolution (km)	Temporal interval	Units
AMSR-E	18 GHz H/V 23 GHz H/V 36 GHz H/V 89 GHz H/V	12	Daily	Kelvin (K)
	Sea ice concentration (SIC)			Percentage (%)
MODIS	Ice surface temperature (IST)	4	Daily	Kelvin (K)
SSM/I	Ice velocity	25	Daily	cm/sec
Fast ice reference data by Fraser, Massom, and Michael (2010)		1	20 days	

2.2. Methods

Figure 1 summarizes the process flow of the fast ice monitoring conducted in this study. A total of 11 input variables were used, including sea ice concentration and eight dual polarization frequency channels from AMSR-E, IST from MODIS, and ice velocity from SSM/I. Since the reference fast ice data were produced from the 20-day MODIS composite images (Fraser, Massom, and Michael 2010), the daily input variables were aggregated into the same 20-day composites using the statistical mean function. During the composite process of the MODIS IST data (MOD29E1D product), the sea ice by reflectance (i.e., sea ice vs. non-sea ice) variable contained in the MODIS IST product was also used to mask out non-sea ice pixels. Variables from the passive microwave sensors were all available for the whole Antarctic region over the study period (i.e., 2003–2008), whereas the IST data were not always available for some areas due to cloud cover during the composite period. Thus, the images <20 could be used in compositing IST data. The input variables used in this study have different spatial resolutions. All input variables and the fast ice reference data were resampled with 4-km resolution using bilinear spatial interpolation.

The sea ice type (i.e., fast ice vs. pack ice) was set to a dependent variable for binary classification. Since the fast ice reference data were only available for the East Antarctic,

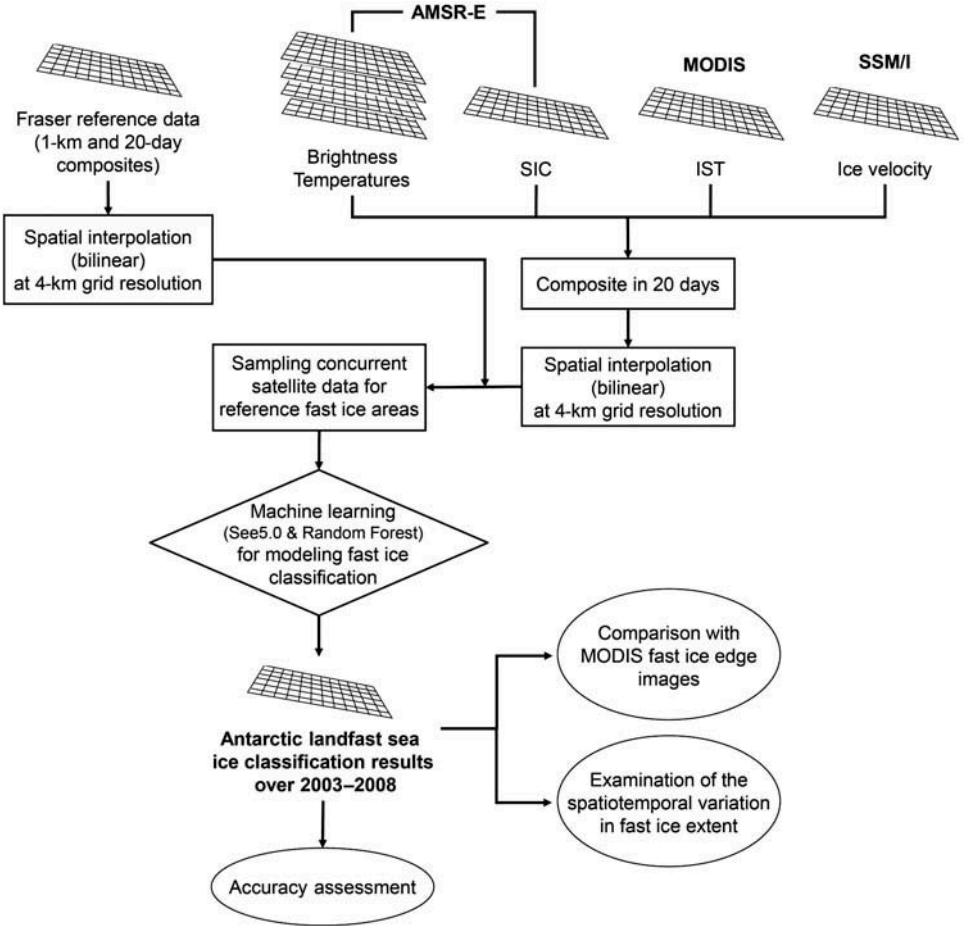

Figure 1. The process flow of the research.

samples to train and validate machine learning-based classification models were extracted only from that region. Within the sea ice extent determined by AMSR-E sea ice concentration data, the area excluding the reference fast ice was considered as pack ice. One million samples (i.e., pixels, approximately 5.2% of the sea ice reference pixels) were selected from the sea ice reference data through stratified sampling as the ratio of 1:4 between fast ice and pack ice for the East Antarctic. Eighty percent of the samples by class were randomly extracted to train the machine learning-based models to classify the sea ice. The remaining 200,000 samples were used as the test data-set to validate the developed models.

Machine learning techniques have been applied to various remote sensing applications including land cover classification, change detection, and biophysical parameter estimation (Maxwell et al. 2014; Ghimire et al. 2012; Li, Im, and Beier 2013; Kim et al. 2014; Long et al. 2013; Rhee, Park, and Lu 2014). Two rule-based machine learning approaches – decision trees (DTs) and random forest (RF) – were used to map fast ice in the Antarctic region. See5.0, a commercial program developed by RuleQuest Research, Inc. (Quinlan 2013), was used to implement DTs. It uses recursive binary splits to extract patterns or rules in a data-set. As See5.0 produces rule-based results (if–then rules), users can interpret the results in a more straightforward and easier way than other methods such as artificial neural networks. RF creates a collection of trees based on Classification and Regression Trees (CART), which is a rule-based DT similar to See5.0 (Breiman 2001). Each tree is grown using two randomizations in selecting training samples and split variables to overcome the limitations of CART, including dependency on a single tree and sensitivity to training samples. A subset of the training samples (typically 67% of the samples) is randomly selected, and the remaining samples (out-of-bag data) are used to internally validate the model. The second randomness is that in each node of a tree, a subset of input variables (typically $\sqrt{n}$ with n as the number of input variables) is randomly selected. The grown trees are then combined using either a simple majority voting or a weighted majority voting strategy. In this study, RF models were developed using an add-on package in R software. All options were set to the default values with 500 as the number of trees. Both machine learning models provide relative variable importance that can be used to examine the contribution of each input variable for fast ice mapping. See5.0 provides attribute usage information that shows how frequently a variable is used at each split. RF provides mean decrease accuracy in classification when a variable is permuted, which means that the greater the decrease in accuracy, the more important the variable is.

To assess the performance of the DT and RF models, confusion matrices produced using the test data-set were examined, including overall accuracy and Kappa coefficient of agreement (Jensen 2005). Furthermore, the time series of fast ice mapping results was compared with all the reference fast ice data over the East Antarctic (Fraser, Massom, and Michael 2010) to calculate the time series of producer's and user's accuracies of fast ice (Equations (1) and (2)).

$$\text{Producer's accuracy} = \frac{OP}{RP} \times 100 \tag{1}$$

$$\text{User's accuracy} = \frac{OP}{MP} \times 100 \tag{2}$$

where OP is the number of overlapping pixels between reference and modeled fast ice, RP is the number of reference fast ice pixels, and MP is the number of modeled fast ice pixels.

As the fast ice reference data were available only for the East Antarctic, additional visual assessment using relatively high-spatial-resolution MODIS images was conducted. National Snow & Ice Data Center (NSIDC)-provided 250-m MODIS Antarctic ice shelf images were used to delineate the fast ice edges based on visual interpretation. Fast ice mapping results of the models were compared with the MODIS-derived fast ice images over selected areas of interest in the Mertz and Abbot Ice Shelf regions in the East and West Antarctic, respectively. While the Mertz region documented relatively slow changing of fast ice distribution, the Abbot region showed rapid change based on the multiyear sea ice information (Massom et al. 2010; Worby et al. 2008).

The spatiotemporal patterns in the fast ice distribution were examined with the 6-year time series of the fast ice extent produced. Two frequency metrics of fast ice occurrence were calculated: the number of switches between occurrence and disappearance of fast ice (1) by pixel and (2) by applying weighted average depending on the number of composites during fast ice residence (Equation (3)).

$$\frac{\sum NC \times n}{\sum n} \tag{3}$$

where NC is the number of composites during fast ice residence, and n is the number of each NC found throughout the study period.

3. Results and discussion

3.1. Fast ice mapping model performance

The Antarctic fast ice mapping models developed by DT and RF were validated using the 200,000 test data-set. The DT and RF models produced similar overall accuracies of 93.09% and 94.77%, respectively (Tables 2 and 3). The RF model resulted in slightly higher performance of sea ice mapping, especially fast ice, than the DT model. The user's and producer's accuracies of pack ice were higher than those of fast ice for both models. This is because the sample size of pack ice was much larger than that of fast ice, and the pack ice samples located far from the coast were easily distinguished from fast ice samples due to a relatively lower sea ice concentration. While the overall accuracy was similar between the two models, the Kappa coefficient of agreement resulted in a greater difference, ~6%, which showed the superiority of RF to DT.

Table 2. Accuracy assessment results for decision trees using the test data-set.

Classified as \ Reference	Fast ice	Pack ice	Sum	User's accuracy
Fast ice	32,274	6099	38,373	84.11%
Pack ice	7726	153,901	161,627	92.22%
Sum	40,000	160,000	200,000	
Producer's accuracy	80.69%	96.19%		
Overall accuracy			93.09%	
Kappa coefficient			78.06%	

Table 3. Accuracy assessment results for random forest using the test data-set.

Classified as \ Reference	Fast ice	Pack ice	Sum	User's accuracy
Fast ice	36,319	6773	43,092	84.28%
Pack ice	3681	153,227	156,908	97.65%
Sum	40,000	160,000	200,000	
Producer's accuracy	90.80%	95.77%		
Overall accuracy			94.77%	
Kappa coefficient			84.13%	

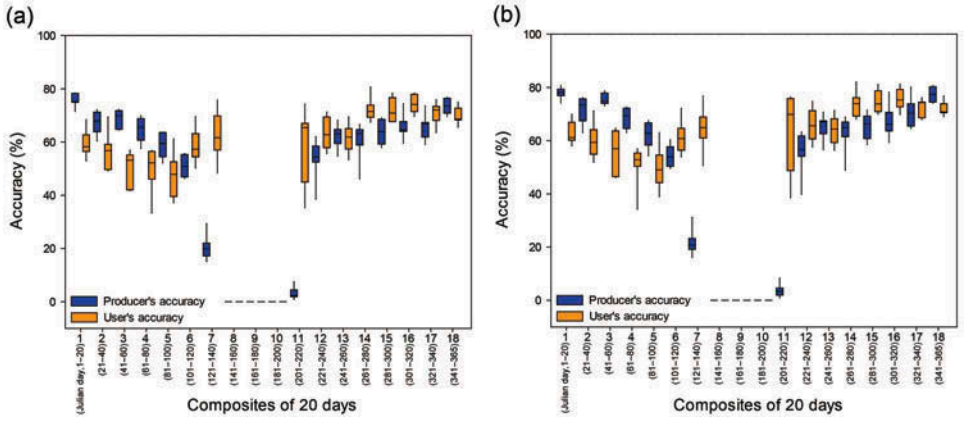

Figure 2. Box plots of the producer's accuracy and user's accuracy for quantitative examination of the fast ice mapping results of (a) decision trees and (b) random forest. For full color versions of the figures in this paper, please see the online version.

The box plots of the producer's and user's accuracies by model calculated using the reference fast ice data-set in the East Antarctic for the entire period (Fraser, Massom, and Michael 2009, 2010) are shown in Figure 2. In Austral winter (composites from 6 to 12), the user's and producer's accuracies of fast ice were significantly low or uncalculated because MODIS IST was not available during the season. Both models produced similar producer's and user's accuracies of fast ice through all composites. RF produced a bit higher accuracy than DT for identifying fast ice. For the first five composites, the producer's accuracy was higher than the user's accuracy for both models, whereas the other composites showed a reversed trend. Both models produced very low producer's accuracy near the winter season (i.e., composites 7 and 11) due to the limited availability of the MODIS IST data.

The relative importance of variables to fast ice mapping for both models is presented in Tables 4 and 5. Ice velocity and IST were the most contributing variables for fast ice classification regardless of the model used. The velocity of fast ice fixed to the shoreline or an ice shelf is close to 0 m/s (Mahoney, Eicken, and Shapiro 2007; Mahoney et al. 2006), whereas pack ice can be easily moved by ocean currents and winds, and thus, it shows larger velocity than fast ice (Heil and Allison 1999). It reveals that ice velocity can be used as a major variable for distinguishing fast ice from pack ice.

Table 4. Attribute usage of the decision trees model.

VEL	IST	SIC	18H	36V	18V	89V	89H	23V	23H	36H
100%	96%	92%	90%	87%	86%	80%	73%	62%	28%	7%

Table 5. Mean decrease accuracy calculated using out-of-bag data when a variable was permuted in random forest. The greater the decrease in accuracy, the more contributing the variable was.

VEL	IST	23V	18H	89H	36V	23H	89V	18V	SIC	36H
607.34	354.89	160.82	160.50	147.04	136.84	111.61	111.40	105.72	103.35	99.53

MODIS IST was identified as the second contributing variable for the fast ice mapping. The IST difference between fast ice and pack ice could be due to the subpixel effects in that fast ice typically has higher ice concentration while pack ice, especially far from the coast, has lower concentration affected by open water at 4 × 4 km resolution (Hall et al. 2001). Open water has a higher surface temperature than sea ice (Hall et al. 2004). Fast ice typically forms at large size, while pack ice is distributed in patches, which results in a relatively higher IST for pack ice. However, the unexpected high IST values over fast ice regions are occasionally found where fast ice is formed for a small area, often occurring in Austral summer (Fraser, Massom, and Michael 2010). IST could also be different between the two types of sea ice due to different physical characteristics. The surface temperature of sea ice depends on the physical properties of sea ice such as emissivity, thickness, and salinity (Hall et al. 2004; Maslanik and Key 1993). Thick sea ice typically has a lower surface temperature than that of thin ice due to its lower emissivity in the infrared bands (Hall et al. 2004). Fast ice can thicken up to a few meters during the ice growing season (Heil, Allison, and Lytle 1996), and thus, it would have a lower surface temperature than the drifting pack ice, which is typically less than 1 m thick (Worby et al. 2008).

While the ice velocity and IST were dominantly important compared to the other variables in the RF model, SIC showed a very high importance rating in the DT model following ice velocity and IST as SIC varies by sea ice type (Comiso, Cavalieri, and Markus 2003). AMSR-E brightness temperatures at 36-GHz, vertically polarized channels and 18-GHz, both vertically and horizontally polarized channels also showed high importance ratings in the DT model, which implies that the brightness temperatures varied depending on sea ice types and ice thickness (Comiso et al. 1997). The three channels have been used to distinguish sea ice types (Comiso et al. 1997). For thick sea ice such as fast ice or multiyear ice, the brightness temperatures are very low ~190 K at 18-GHz H and 36-GHz V channels and 220 K at the 18-GHz V channel, while thin first-year ice such as pack ice and drift ice radiates much higher brightness temperatures at the three channels (~240 K at the 18 GHz H and 36 GHz V; and ~250 K at 18 GHz V) than thick sea ice (Comiso et al. 1997). In addition, as 89-GHz channels are less affected by snow or ice layers on sea ice than 36- and 18-GHz channels under clear sky conditions, 89-GHz channels can be used to differentiate the types of sea ice on which snow or ice accumulates (Markus and Cavalieri 2000).

The contribution of the brightness temperatures measured at the other AMSR-E channels to the sea ice classification was relatively low, especially at 36 GHz H, showing the

lowest importance for both models. This is because the 36-GHz H channel is sensitive to changes in atmospheric water vapor content instead of sea ice properties (Maslanik 1992).

3.2. *Comparison with MODIS images*

Fast ice mapping results from the DT and RF models were compared with the fast ice area extracted from MODIS images with 250-m spatial resolution (band 2) over the Mertz Ice Shelf region in the East Antarctic and Abbot Ice Shelf in the West Antarctic with different periods considering the variability of fast ice (Figures 3 and 4). When the fast ice near

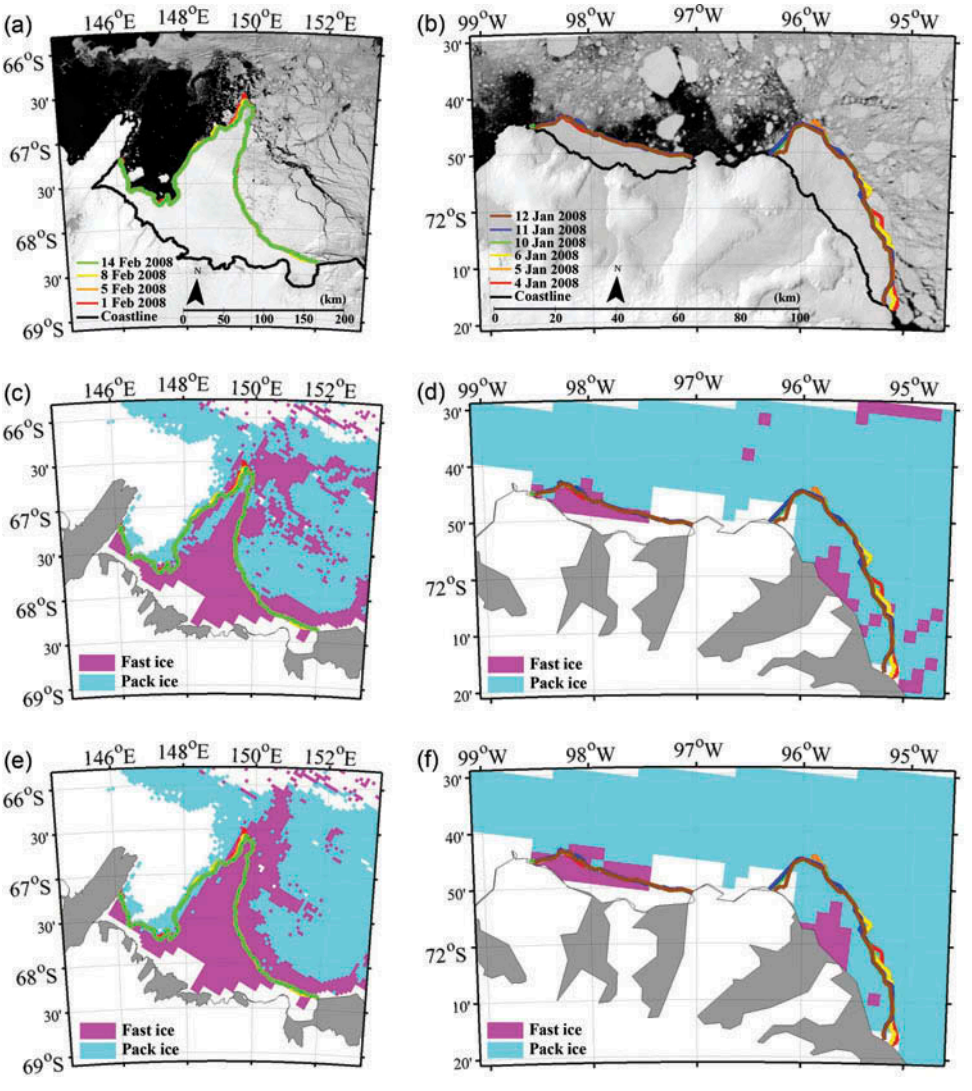

Figure 3. Comparison of fast ice mapping results by model with the 250-m MODIS images during the periods of relatively stable fast ice around (a) Mertz and (b) Abbot Ice Shelf in the East and West Antarctica, respectively. The lines in (a) and (b) indicate fast ice edges delineated from the MODIS images based on visual interpretation. Decision tree results are shown in (c) and (d), while random forest results are in (e) and (f). MODIS images with the maximum fast ice cover were used as background images in (a) and (b).

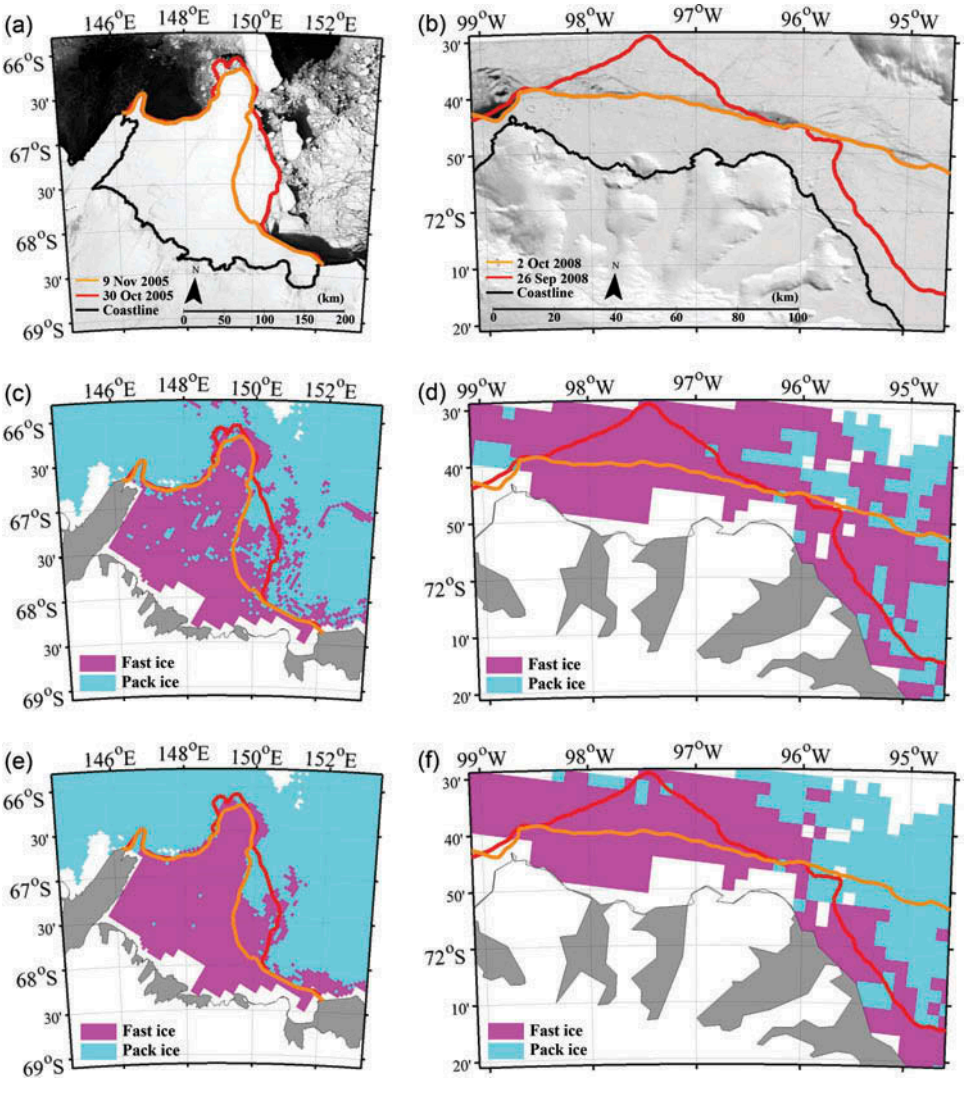

Figure 4. Comparison of fast ice mapping results by model with the 250-m MODIS images during the periods of rapidly changing fast ice around (a) Mertz and (b) Abbot Ice Shelf in the East and West Antarctica, respectively. The lines in (a) and (b) indicate fast ice edges delineated from the MODIS images based on visual interpretation. Decision tree results are shown in (c) and (d), while random forest results are in (e) and (f). MODIS images with the maximum fast ice cover were used as background images in (a) and (b).

Mertz Ice Shelf was relatively stable during 13 days of the MODIS images (Figure 3a), the RF model detected fast ice better than DT compared with the actual fast ice areas (Figures 3c and 3e). This might be because the RF model used the ice velocity and IST much more significantly than DT to classify ice types compared to the other variables, such as the brightness temperatures at 18 GHz H and V and 36 GHz V. For example, wide ice floes located to the right of the fast ice appeared to be dropped out of the fast ice, and thus, they had reflectivity and morphology similar to the fast ice. Therefore, the

microwave radiation properties, i.e., the brightness temperature, of the ice floes were similar to those of the fast ice (not shown). It resulted in misclassification between the fast ice and ice floes when the DT model with high importance of the brightness temperatures at 18 GHz H and V and at 36 GHz V was used. Since the ice floes and fast ice had different ice velocity and IST values, RF was able to identify the fast ice in the region relatively better than DT.

For the relatively stable fast ice during 8 days in Abbot Glacier in the West Antarctica (Figure 3b), both the DT (Figure 3d) and RF (Figure 3f) models mapped much smaller fast ice areas than the actual fast ice areas. The low spatial resolution of the passive microwave-derived variables (12–25 km) could be a major reason as the fast ice was very narrowly attached to the shoreline. In addition, MODIS IST with relatively higher spatial resolution was not always available for the period of the corresponding composite due to heavy clouds (i.e., ~25% available on average), which resulted in very limited examination of the temporal variation of the fast ice areas.

Previous studies reported that the 20-day compositing period well represented the variation, growth, and breakup of fast ice, and thus, it is enough to map fast ice areas in the polar region (Fraser, Massom, and Michael 2010; Mahoney et al. 2006). However, substantial changes in the fast ice areas in 20 days were often observed in both the East and West Antarctic from the MODIS images (Figure 4). This implies that the 20-day composite interval might not be sufficient to represent the variation of fast ice, especially where it rapidly changes over a short period of time. For such areas, fast ice should be monitored with a compositing period less than 20 days. For the rapidly changing period around Mertz (Figure 4a) and Abbot Ice Shelf (Figure 4b), the performance of the RF (Figure 4e and 4f) model was slightly better than DT (Figure 4c and 4d) through the visual validation of the fast ice mapping results with the high-resolution MODIS images. This also corresponds to the accuracy assessment results of the classification models (Tables 2 and 3).

3.3. Spatiotemporal variation of fast ice in the East and West Antarctic

As the RF model produced better fast ice classification results than the DT model, the RF-derived maps were used to examine the spatiotemporal variation of fast ice. Fast ice in the entire Antarctic Ocean was mapped by composite period (i.e., 20 days) from 2003 to 2008. Although MODIS IST was identified as one of the most important variables to detect fast ice, it has a major drawback, which is its limited availability. Due to the lack of MODIS IST data during the Australian winter season, fast ice mapping results could not be obtained for the sixth (101–120 Julian days) to twelfth (221–240 Julian days) composite periods. Figure 5 shows the distribution maps of fast ice produced by the RF model for two composites in 2003. Hatched areas in Figure 5 represent that IST was not available during the composite period, which resulted in no fast ice classified in the areas. The limited spatial coverage of IST could increase uncertainty of fast ice distribution in the Antarctic. As shown in Figure 6, the spatial discontinuity of IST data was larger in the West Antarctica than in the East throughout the entire composite period. While the availability of IST is higher in the East Antarctica than in the West, some regions in the East Antarctica also had no available IST data for a certain time of period.

The time series of fast ice extent is depicted for the East and West Antarctica between 2003 and 2008 in Figure 7. While the temporal variation of the fast ice areas in the West Antarctica appeared higher than that in the East (with standard deviations of 122,457 km^2

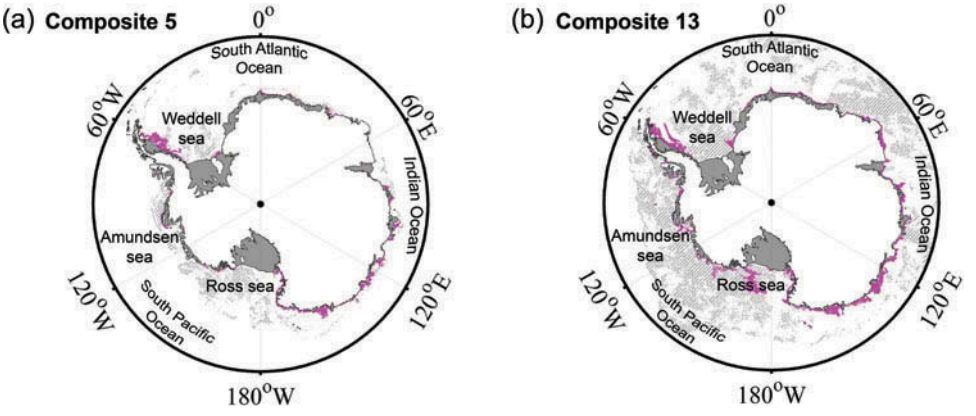

Figure 5. Fast ice maps using random forest in 2003 for (a) composite 5 (81–100 Julian days) and (b) composite 13 (241–260 Julian days). Magenta areas represent fast ice in the Antarctic, and hatched areas with gray color indicate that MODIS IST was not available for the composite.

in the West Antarctica and 69,158 km^2 in the East), it should be noted that the limited availability of IST data might increase temporal uncertainty in the fast ice distribution especially around Weddell Sea and Ross Sea in the West Antarctica. Fraser et al. (2012) reported that the fast ice extent maximum was found around September and the minimum around March in the East Antarctica. Our results for the East Antarctica also showed a similar trend (Figure 7). However, such a pattern was not found for the West Antarctica, possibly due to the data void problem caused by MODIS IST data. Unlike the East Antarctica, many data voids occurred along the coast especially in the Weddell Sea and Ross Sea in the West Antarctica, which significantly increased the uncertainty of the fast ice distribution in those regions. No training data from the West Antarctica were used in the classification models, which possibly increased the false alarm or false negatives of the fast ice detection to lead to the increase in the uncertainty of the fast ice distribution. Consequently, the temporal (seasonal and annual) variation of fast ice distribution in the West Antarctica should deserve further research.

Figure 8 shows the distribution of the frequency of fast ice residence using simple counting of the switches (i.e., occurrence and disappearance) and the weighted average approach (Equation (3)). In order to mitigate the data void problem, it was excluded in the frequency calculation when a pixel in a composite had no data. High values of frequency for the simple counting approach indicated that the advance and retreat of fast ice frequently occurred during the study period. While the temporal variation of the fast ice based on the simple counting approach was generally high in the edge of fast ice all over the East Antarctica, it was only high for specific areas such as Weddell and Amundsen Sea in the West Antarctica (Figure 8a). When the weighted average approach was used, high values meant that the fast ice residence time was relatively long, while low values indicated that fast ice only existed for a short period of time (Figure 8b). While the weighted average of the fast ice residence was very low in the West Antarctica, it was relatively high in the East Antarctica, which corresponds to more gradual change of fast ice distribution in the East Antarctic region (Figure 7).

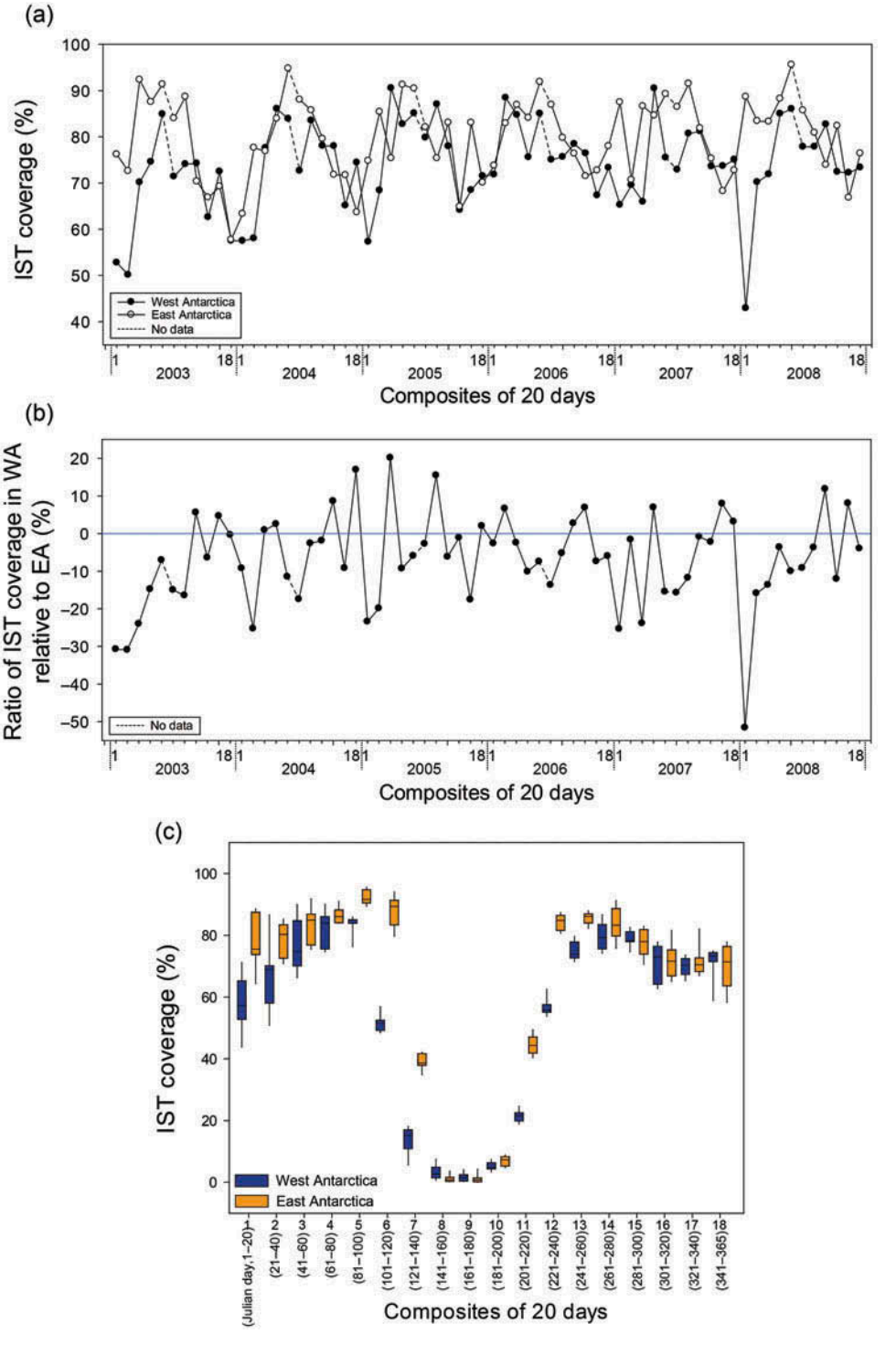

Figure 6. (a) Temporal variation of the availability of MODIS IST data in the East and West Antarctic regions. (b) The ratio of the IST coverage in the West Antarctic (WA) relative to the East Antarctic (EA) in percentage. (c) Box plot of the IST coverage in percentage by composite.

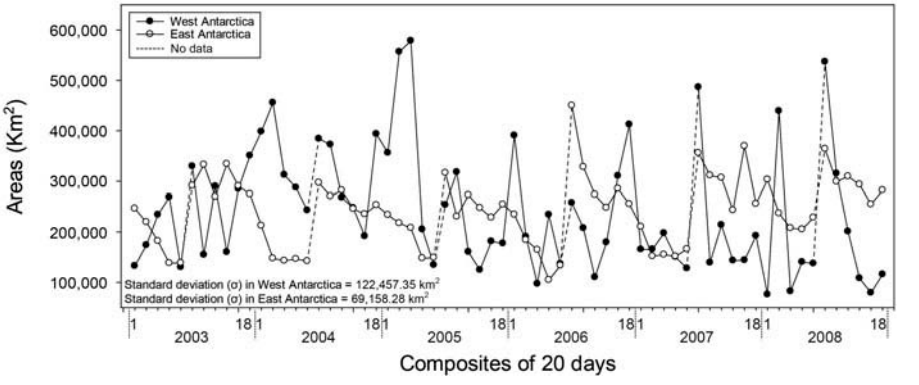

Figure 7. Temporal variation of fast ice areas in the East and West Antarctic. Due to the lack of the input data during the Australian winter season, composites 6–12 for each year were not available.

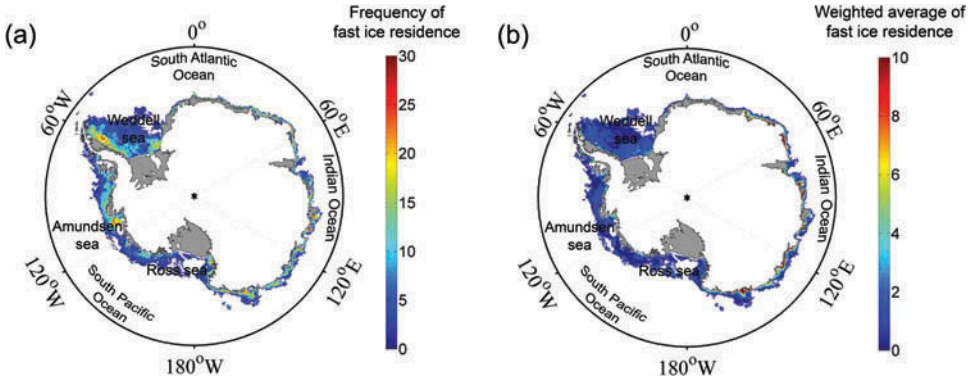

Figure 8. Temporal variation of fast ice in the Antarctic using (a) the simple counting approach and (b) the weighted average approach.

4. Conclusions

In this study, fast ice in the East and West Antarctic was mapped using multisensor data and machine learning techniques – DT and RF – during the period from 2003 to 2008. RF produced better performance than DT for fast ice mapping based on the accuracy assessment and visual interpretation of the classification maps in conjunction with 250-m MODIS images. Ice velocity and IST were identified as the most contributing variables to classify fast ice regardless of the approach used. Based on the time series of the fast ice maps produced by RF, the spatiotemporal variations of fast ice were examined over the entire Antarctic. While the temporal pattern of fast ice extent for the East Antarctica agreed with the literature, no clear pattern was found for the West Antarctica due to the data void problem, which resulted in considerable uncertainty of the fast ice distribution. Fast ice residence time was relatively long in the East Antarctica, which indicates gradual changes in advance and retreat of fast ice. However, fast ice residence time was very short in the West Antarctica partially due to the no-data pixels from MODIS IST data.

Since some areas had a high variation of fast ice for a short period of time, composting of input variables with a period of less than 20 days is necessary to accurately monitor fast ice in the Antarctic. However, since MODIS IST, one of the most contributing variables, is heavily influenced by clouds, the number of no-data pixels inevitably increases when compositing IST with a small number of days (e.g., 10 days). Thus, spatial and temporal interpolation might be necessary to solve the data void problem when using a small number of days for compositing of MODIS IST. Future research includes (1) incorporating additional variables such as CryoSat-2-derived sea ice thickness for fast ice mapping to improve classification accuracy and (2) linking time series of fast ice distribution to climate change indicators to better understand the Antarctic climate system and its relation to other regional climate systems.

Acknowledgment

Special thanks to Dr Alexander Fraser for sharing the fast ice maps of the East Antarctic for reference.

Disclosure statement

No potential conflict of interest was reported by the authors.

Funding

This research was supported by the project titled "SaTellite remote sensing on set Antarctic ocean Research (STAR) [KOPRI, PE15040]", funded by the Korea Polar Research Institute, South Korea, and was partially supported by the Space Core Technology Development program through the National Research Foundation of Korea funded by the Ministry of Science, ICT and Future Planning (2014M1A3A3A03034799).

References

Breiman, L. 2001. "Decision-Tree Forests." *Machine Learning* 45 (1): 5–32. doi:10.1023/A:1010933404324.

Cavalieri, D. J. 1991. "Aircraft Active and Passive Microwave Validation of Sea Ice Concentration From the Defense Meteorological Satellite Program Special Sensor Microwave Imager." *Journal of Geophysical Research: Oceans (1978–2012)* 96 (C12): 21989–22008. doi:10.1029/91JC02335.

Cavalieri, D. J., T. Markus, and J. C. Comiso. 2014. *AMSR-E/Aqua Daily L3 12.5 km Brightness Temperature, Sea Ice Concentration, & Snow Depth Polar Grids*. Version 3. 2003–2008. Boulder, CO: NASA DAAC at the National Snow and Ice Data Center. doi:10.5067/AMSR-E/AE_SI12.003.

Comiso, J. C., D. J. Cavalieri, and T. Markus. 2003. "Sea Ice Concentration, Ice Temperature, and Snow Depth Using AMSR-E Data." *IEEE Transactions on Geoscience and Remote Sensing* 41 (2): 243–252. doi:10.1109/TGRS.2002.808317.

Comiso, J. C., D. J. Cavalieri, C. L. Parkinson, and P. Gloersen. 1997. "Passive Microwave Algorithms for Sea Ice Concentration: A Comparison of Two Techniques." *Remote Sensing of Environment* 60 (3): 357–384. doi:10.1016/S0034-4257(96)00220-9.

Fedotov, V. I., N. V. Cherepanov, and K. P. Tyshko. 1998. "Some Features of the Growth, Structure and Metamorphism of East Antarctic Landfast Sea Ice." In *Antarctic Sea Ice: Physical Processes, Interactions and Variability*, edited by M. O. Jeffries. Washington, DC: American Geophysical Union. doi:10.1029/AR074p0343.

Fowler, C., W. Emery, and M. Tschudi. 2013. *Polar Pathfinder Daily 25 km EASE-Grid Sea Ice Motion Vectors*. Version 2. 2003–2008. Boulder, CO: National Snow and Ice Data Center.

Fraser, A. D. 2011. "East Antarctic Landfast Sea-ice Distribution and Variability." PhD thesis, University of Tasmania.

Fraser, A. D., R. A. Massom, and K. J. Michael. 2009. "A Method for Compositing Polar MODIS Satellite Images to Remove Cloud Cover for Landfast Sea-Ice Detection." *IEEE Transactions on Geoscience and Remote Sensing* 47 (9): 3272–3282. doi:10.1109/TGRS.2009.2019726.

Fraser, A. D., R. A. Massom, and K. J. Michael. 2010. "Generation of High-Resolution East Antarctic Landfast Sea-Ice Maps from Cloud-Free MODIS Satellite Composite Imagery." *Remote Sensing of Environment* 114 (12): 2888–2896. doi:10.1016/j.rse.2010.07.006.

Fraser, A. D., R. A. Massom, K. J. Michael, B. K. Galton-Fenzi, and J. L. Lieser. 2012. "East Antarctic Landfast Sea Ice Distribution and Variability, 2000–08." *Journal of Climate* 25 (4): 1137–1156. doi:10.1175/JCLI-D-10-05032.1.

Ghimire, B., J. Rogan, V. R. Galiano, P. Panday, and N. Neeti. 2012. "An Evaluation of Bagging, Boosting, and Random Forests for Land-Cover Classification in Cape Cod, Massachusetts, USA." *GIScience & Remote Sensing* 49 (5): 623–643. doi:10.2747/1548-1603.49.5.623.

Giles, A. B., R. A. Massom, and V. I. Lytle. 2008. "Fast-Ice Distribution in East Antarctica during 1997 and 1999 Determined Using RADARSAT Data." *Journal of Geophysical Research: Oceans (1978–2012)* 113 (C2). doi:10.1029/2007JC004139.

Hall, D. K., J. R. Key, K. A. Casey, G. A. Riggs, and D. J. Cavalieri. 2004. "Sea Ice Surface Temperature Product from MODIS." *IEEE Transactions on Geoscience and Remote Sensing* 42 (5): 1076–1087. doi:10.1109/TGRS.2004.825587.

Hall, D. K., G. A. Riggs, V. V. Salomonson, J. S. Barton, K. Casey, J. Y. L. Chien, N. E. DiGirolamo, A. G. Klein, H. W. Powell, and A. B. Tait. 2001. "Algorithm Theoretical Basis Document (ATBD) for the MODIS Snow and Sea Ice-Mapping Algorithms." http://modis.gsfc.nasa.gov/data/atbd/atbd_mod10.pdf.

Hall, D. K., V. V. Salomonson, and G. A. Riggs. 2006. *MODIS/Aqua Sea Ice Extent and IST Daily L3 Global 4km EASE-Grid Day.* Version 5. 2003–2008. Boulder, CO: National Snow and Ice Data Center.

Heil, P. 2006. "Atmospheric Conditions and Fast Ice at Davis, East Antarctica: A Case Study." *Journal of Geophysical Research: Oceans (1978–2012)* 111 (C5). doi:10.1029/2005JC002904.

Heil, P., and I. Allison. 1999. "The Pattern and Variability of Antarctic Sea-Ice Drift in the Indian Ocean and Western Pacific Sectors." *Journal of Geophysical Research: Oceans (1978–2012)* 104 (C7): 15789–15802. doi:10.1029/1999JC900076.

Heil, P., I. Allison, and V. I. Lytle. 1996. "Seasonal and Interannual Variations of the Oceanic Heat Flux under a Landfast Antarctic Sea Ice Cover." *Journal of Geophysical Research-Oceans* 101 (C11): 25741–25752. doi:10.1029/96JC01921.

Heil, P., S. Gerland, and M. A. Granskog. 2011. "An Antarctic Monitoring Initiative for Fast Ice and Comparison with the Arctic." *The Cryosphere Discussions* 5 (5): 2437–2463. doi:10.5194/tcd-5-2437-2011.

Jensen, J. R. 2005. *Introductory Digital Image Processing: A Remote Sensing Perspective*. 3rd ed. Upper Saddle River, NJ: Prentice-Hall.

Kim, Y. H., J. H. Im, H. K. Ha, J. K. Choi, and S. H. Ha. 2014. "Machine Learning Approaches to Coastal Water Quality Monitoring Using GOCI Satellite Data." *GIScience & Remote Sensing* 51 (2): 158–174. doi:10.1080/15481603.2014.900983.

Lei, R., Z. Li, B. Cheng, Z. Zhang, and P. Heil. 2010. "Annual Cycle of Landfast Sea Ice in Prydz Bay, East Antarctica." *Journal of Geophysical Research: Oceans* 115 (C2): C02006. doi:10.1029/2008JC005223.

Li, M., J. H. Im, and C. Beier. 2013. "Machine Learning Approaches for Forest Classification and Change Analysis Using Multi-Temporal Landsat TM Images over Huntington Wildlife Forest." *GIScience & Remote Sensing* 50 (4): 361–384.

Long, J. A., R. L. Lawrence, M. C. Greenwood, L. Marshall, and P. P. Miller. 2013. "Object-Oriented Crop Classification Using Multitemporal ETM+ SLC-Off Imagery and Random Forest." *GIScience & Remote Sensing* 50 (4): 418–436.

Mahoney, A., H. Eicken, A. G. Gaylord, and L. Shapiro. 2007. "Alaska Landfast Sea Ice: Links with Bathymetry and Atmospheric Circulation." *Journal of Geophysical Research: Oceans* 112 (C2): C02001. doi:10.1029/2006JC003559.

Mahoney, A., H. Eicken, and L. Shapiro. 2007. "How Fast Is Landfast Sea Ice? A Study of the Attachment and Detachment of Nearshore Ice at Barrow, Alaska." *Cold Regions Science and Technology* 47 (3): 233–255. doi:10.1016/j.coldregions.2006.09.005.

Mahoney, A., H. Eicken, L. Shapiro, and A. Graves. 2006. "Defining and Locating the Seaward Landfast Ice Edge in Northern Alaska." 18th International Conference on Port and Ocean Engineering under Arctic Conditions (POAC'05), Potsdam, NY, June 26–30, 2005.

Markus, T., and D. J. Cavalieri. 2000. "An Enhancement of the NASA Team Sea Ice Algorithm." *IEEE Transactions on Geoscience and Remote Sensing* 38 (3): 1387–1398. doi:10.1109/36.843033.

Maslanik, J. 1992. "Effects of Weather on the Retrieval of Sea Ice Concentration and Ice Type from Passive Microwave Data." *International Journal of Remote Sensing* 13 (1): 37–54. doi:10.1080/01431169208904024.

Maslanik, J., and J. Key. 1993. "Comparison and Integration of Ice-Pack Temperatures Derived Front A VHRR and Passive Nticrowave Intagery." *Annals of Glaciology* 17: 372–378.

Massom, R. A., A. B. Giles, H. A. Fricker, R. C. Warner, B. Legrésy, G. Hyland, N. Young, and A. D. Fraser. 2010. "Examining the Interaction between Multi-Year Landfast Sea Ice and the Mertz Glacier Tongue, East Antarctica: Another Factor in Ice Sheet Stability?" *Journal of Geophysical Research* 115 (C12): C12027. doi:10.1029/2009JC006083.

Massom, R. A., K. Hill, C. Barbraud, N. D. Adams, A. Ancel, L. Emmerson, and M. J. Pook. 2009. "Fast Ice Distribution in Adélie Land, East Antarctica: Interannual Variability and Implications for Emperor Penguins Aptenodytes Forsteri." *Marine Ecology Progress Series* 374 (January): 243–257. doi:10.3354/meps07734.

Maxwell, A. E., M. P. Strager, T. A. Warner, N. P. Zégre, and C. B. Yuill. 2014. "Comparison of NAIP Orthophotography and RapidEye Satellite Imagery for Mapping of Mining and Mine Reclamation." *GIScience & Remote Sensing* 51 (3): 301–320.

Meyer, F. J., A. R. Mahoney, H. Eicken, C. L. Denny, H. C. Druckenmiller, and S. Hendricks. 2011. "Mapping Arctic Landfast Ice Extent Using L-Band Synthetic Aperture Radar Interferometry." *Remote Sensing of Environment* 115 (12): 3029–3043. doi:10.1016/j.rse.2011.06.006.

Quinlan, R. 2013. "See5.0: An Informal Tutorial." Accessed May 26, 2014. http://www.rulequest.com

Rhee, J. Y., S. Y. Park, and Z. Lu. 2014. "Relationship between Land Cover Patterns and Surface Temperature in Urban Areas." *GIScience & Remote Sensing* 51 (5): 521–536. doi:10.1080/15481603.2014.964455.

Spreen, G., L. Kaleschke, and G. Heygster. 2008. "Sea Ice Remote Sensing Using AMSR-E 89-Ghz Channels." *Journal of Geophysical Research: Oceans (1978–2012)* 113 (C2). doi:10.1029/2005JC003384.

Tamura, T., K. I. Ohshima, T. Markus, D. J. Cavalieri, S. Nihashi, and N. Hirasawa. 2007. "Estimation of Thin Ice Thickness and Detection of Fast Ice from SSM/I Data in the Antarctic Ocean." *Journal of Atmospheric and Oceanic Technology* 24 (10): 1757–1772. doi:10.1175/JTECH2113.1.

Tang, S., D. Qin, J. Ren, J. Kang, and Z. Li. 2007. "Structure, Salinity and Isotopic Composition of Multi-Year Landfast Sea Ice in Nella Fjord, Antarctica." *Cold Regions Science and Technology* 49 (2): 170–177. doi:10.1016/j.coldregions.2007.03.005.

Ushio, S. 2006. "Factors Affecting Fast-Ice Break-Up Frequency in Lützow-Holm Bay, Antarctica." *Annals of Glaciology* 44 (1): 177–182. doi:10.3189/172756406781811835.

Worby, A. P., C. A. Geiger, M. J. Paget, M. L. V. Woert, S. F. Ackley, and T. L. DeLiberty. 2008. "Thickness Distribution of Antarctic Sea Ice." *Journal of Geophysical Research: Oceans (1978–2012)* 113 (C5). doi:10.1029/2007JC004254.